

Computational modelling of the piglet brain to simulate near-infrared spectroscopy and magnetic resonance spectroscopy data collected during oxygen deprivation

Tracy Moroz^{1,2,*}, Murad Banaji⁴, Nicola J. Robertson³,
Chris E. Cooper⁵ and Ilias Tachtsidis²

¹CoMPLEX, ²Department of Medical Physics and Bioengineering, and ³Institute for Women's Health, University College London, London, UK

⁴Department of Mathematics, University of Portsmouth, Portsmouth, UK

⁵Department of Biological Sciences, University of Essex, Colchester, UK

We describe a computational model to simulate measurements from near-infrared spectroscopy (NIRS) and magnetic resonance spectroscopy (MRS) in the piglet brain. Piglets are often subjected to anoxic, hypoxic and ischaemic insults, as experimental models for human neonates. The model aims to help interpret measurements and increase understanding of physiological processes occurring during such insults. It is an extension of a previous model of circulation and mitochondrial metabolism. This was developed to predict NIRS measurements in the brains of healthy adults i.e. concentration changes of oxyhaemoglobin and deoxyhaemoglobin and redox state changes of cytochrome c oxidase (CCO). We altered and enhanced the model to apply to the anaesthetized piglet brain. It now includes metabolites measured by ³¹P-MRS, namely phosphocreatine, inorganic phosphate and adenosine triphosphate (ATP). It also includes simple descriptions of glycolysis, lactate dynamics and the tricarboxylic acid (TCA) cycle. The model is described, and its simulations compared with existing measurements from piglets during anoxia. The NIRS and MRS measurements are predicted well, although this requires a reduction in blood pressure auto-regulation. Predictions of the cerebral metabolic rate of oxygen consumption (CMRO₂) and lactate concentration, which were not measured, are given. Finally, the model is used to investigate hypotheses regarding changes in CCO redox state during anoxia.

Keywords: NIRS; MRS; mathematical model; neonatal

1. INTRODUCTION

In preclinical neonatology research, piglets are often used as experimental models for human neonates. At birth, their brains have a similar level of maturity to that of human brains [1]. Many studies have used piglets to help understand the effects of oxygen deprivation on cerebral blood flow and metabolism [2,3]. Piglets have also been used to investigate encephalopathy following hypoxia–ischaemia (HI), a major cause of perinatal brain injury [4]. One review found 23 per cent of 292 animal studies of perinatal hypoxic ischaemic encephalopathy had used piglets [5].

The physiological response of the brain during insults such as HI is complex. To help understand it, we have adopted a systems biology approach, and thus developed

a mathematical model of circulation and metabolism in the neonatal piglet brain. The model has been created by extending and adapting previous physiological models of the brain [6,7]. Like these, it includes a biophysical sub-model of blood flow on a macroscopic scale, linked to a biochemical sub-model of cellular metabolism. We aim to use the model to help interpret experimental measurements, in particular, non-invasive measurements from near-infrared spectroscopy (NIRS) and magnetic resonance spectroscopy (MRS), both of which have been used extensively in piglet studies.

NIRS uses light to measure concentration changes of oxyhaemoglobin and deoxyhaemoglobin in the blood [8]. Changes in the total haemoglobin concentration in the brain correspond to changes in cerebral blood volume. NIRS has a variety of clinical applications [9], and has frequently been used to study the newborn brain [10].

NIRS can also monitor redox changes at the Cu_A centre of cytochrome c oxidase (CCO). The difficulty

*Author for correspondence (t.moroz@ucl.ac.uk).

Electronic supplementary material is available at <http://dx.doi.org/10.1098/rsif.2011.0766> or via <http://rsif.royalsocietypublishing.org>.

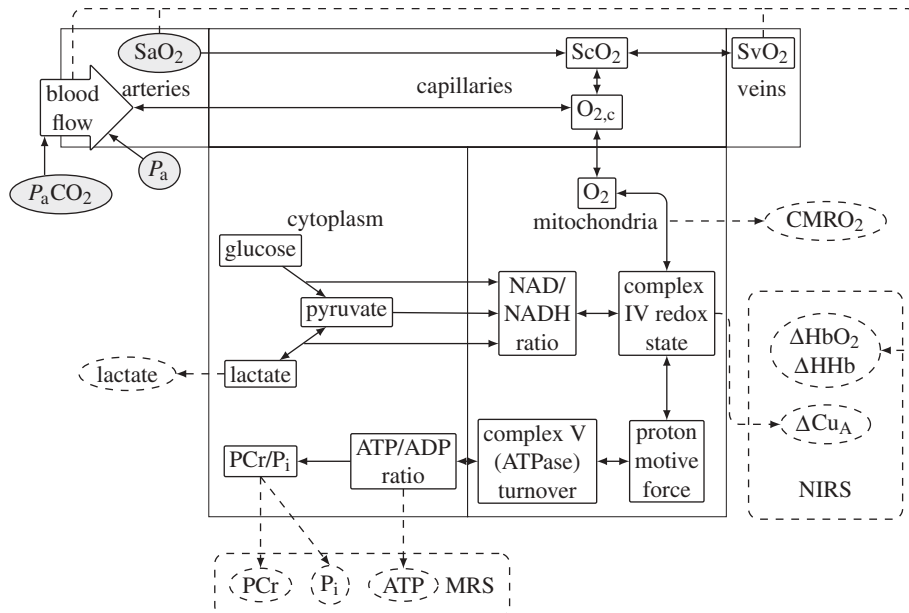


Figure 1. Schematic of the model showing compartments and important variables. Inputs are shown in shaded ovals, outputs in dashed ovals and model variables in rectangles.

in interpreting the NIRS Cu_A measurement was the main motivation for the development of a previous model by Banaji *et al.* [7], which we will refer to as BrainSignals. We have used this as the basis of our piglet model, since we also aim to investigate interpretation of the Cu_A signal. CCO is responsible for oxygen consumption in mitochondrial respiration; therefore, the redox state of Cu_A changes with mitochondrial oxygen tension. However, it is also affected by other factors such as adenosine triphosphate (ATP) and adenosine diphosphate (ADP) concentrations.

MRS uses the principle of nuclear magnetic resonance to measure the concentrations of a range of metabolites [11]. Several different nuclei can be measured including ³¹P and ¹H. ³¹P MRS measures concentrations of the phosphorus-containing metabolites ATP, inorganic phosphate (P_i) and phosphocreatine (PCr). ADP is not present at high enough concentrations to be measurable. Among the metabolites detectable by proton MRS are lactate and N-acetyl-aspartate.

In this paper, we (i) describe our new development of a piglet brain model, and its addition of simulating the MRS measurable concentrations of lactate, PCr, ATP and ³¹P; (ii) test the model by comparing its simulations of anoxia with experimental results from Springett *et al.* [12] involving simultaneous NIRS and ³¹P MRS measurements; (iii) present hypotheses regarding the interpretation of the reduction in CCO observed during anoxia in these experiments, and the subsequent hyperoxidation during the resuscitation phase; and (iv) predict CMRO₂ and lactate concentrations, which were not measured, and propose a hypothesis regarding brain autoregulation in 1-day old piglets.

2. METHODS

A schematic diagram of the model is shown in figure 1. It was based on BrainSignals [7], a model designed to

simulate NIRS signals in the healthy adult brain. It was adapted to the neonatal piglet brain by changing the values of appropriate parameters. Of the 107 explicitly set numerical parameters in our model, 78 are taken from BrainSignals, and 11 of their values have been changed as shown in table 1. As well as these parameter changes, the model was expanded from BrainSignals to simulate variables that are measured by MRS. These include the ³¹P MRS measured variables ATP, PCr and P_i, and the lactate concentration measured by ¹H MRS.

The approach for this model expansion followed the approach taken in BrainSignals i.e. the model was constructed to represent the underlying physiology. However, processes that are not commonly followed by non-invasive measurements necessarily require simplification to prevent the model from becoming overly complicated. Therefore, some processes and parameters are included which are chosen to fit relevant experimental data. The expansion required the addition of 29 numerical parameters shown in table 2. Where possible, these were set from experimental measurements, but some values were taken from other models. In addition, several rate constants were set by flux balance analysis, subject to the constraints of the explicitly set parameter values. A description of the piglet model is given below, concentrating on those aspects that differ from, or are additional to BrainSignals. Full details of the piglet model can be found on the model website [34].

2.1. Circulation

The circulatory part of the model comprises three compartments: arteries and arterioles, capillaries and veins. The arterial and venous compartments have variable volumes V_a and V_v , normalized such that the sum of their normal values ($V_{a,n}$ and $V_{v,n}$) is 1. For simplicity, the volume of the capillaries is ignored, as it is assumed to be small [35]. The arterial/arteriolar compartment

Table 1. Table of parameters from BrainSignals with values changed to represent the anaesthetized piglet brain.

parameter	description	units	BrainSignals	piglet	source
CBF _n	normal CBF	ml 100 g ⁻¹ min ⁻¹	49	46	[13]
[CCO] _{tis}	total CCO concentration in tissue	μM	5.5	2.2	[14,15]
Cu _{A,frac,n}	normal fraction of CCO oxidized		0.80	0.67	[15]
CMRO _{2,n}	normal CMRO ₂	mol 100 g ⁻¹ min ⁻¹	155	114	[13,16]
P _a and P _{a,n}	mean arterial blood pressure	mmHg	100	50	[13]
[Hbtot] and [Hbtot] _n	total blood haemoglobin conc	mM (×4)	9.1	5.4	[17]
V _{blood,n}	normal brain blood fraction		0.0400	0.0325	[16]
P _{ic} and P _{ic,n}	intracranial pressure	mmHg	9.5	4.5	[18]

Table 2. Table of new model parameters.

parameter	value	source
[ADP] _n	0.012 mM	[19]
[PCr] _n	2.6 mM	[20]
[ATP] _n	2.2 mM	[20]
[Py] _n	0.1 mM	[1]
[gluc] _n	1.2 mM	[21]
[gluc] _c	5.3 mM	[15]
[lac] _n	3.0 mM	[22]
[lac] _c	2.0 mM	[15]
[PCr] _n /[Pi] _n	1.5	[14,23]
n _a	4.33	[24]
k _{m,ATP}	0.025	[25]
k _{PCr}	111 mM ⁻¹ s ⁻¹	^a
K _{eq, PCr}	166	[26]
CMR _{gluc,n}	25 μmol min ⁻¹ 100g ⁻¹	[27]
k _{glut}	6.2 mM	[28]
k _{MCT}	2.0 mM	[21]
P _{vs}	1.5 mmHg	[29]
G _{VArat,n}	4	[30]
k _{m,glycG}	0.05 mM	[31]
k _{m,glycA}	0.2 × [ADP] _n	[6]
k _{m,glycP}	0.2 × [P] _n	[6]
I	3	[6]
C _v	0.047 mmHg ⁻¹	[6]
k _{pl}	10 s ⁻¹	^a
k _{AK}	1055 s ⁻¹ mM ⁻¹	[6,25]
k _{AK} ⁻	379 s ⁻¹ mM ⁻¹	[6,25]
k _{m,tcaP}	0.005 × [Py] _n	[32]
k _{m,tcaN}	0.6 × [NAD] _n	[32]
ΔG°	-30.5 kJ mol ⁻¹	[33]

^aRate constants set to give fast reactions compared with other changes.

has a variable conductance G which is sensitive to four inputs: the capillary oxygen concentration $[O_{2,c}]$, the mean arterial blood pressure P_a , the arterial pressure of carbon dioxide P_aCO_2 , and a parameter representing neuronal activation. The oxygen concentration affects conductance via the following equations.

$$\frac{dv_{O_2}}{dt} = \frac{1}{\tau_{O_2}} ([O_{2,c}] - v_{O_2}) \quad (2.1)$$

and

$$\eta = R_O \left(\frac{v_{O_2}}{v_{O_{2,n}}} - 1 \right) + \dots \quad (2.2)$$

Here, τ_{O_2} is a time constant and v_{O_2} represents a low-pass filtered version of $[O_{2,c}]$ with normal value $v_{O_{2,n}}$.

R_O is a parameter controlling the magnitude of the response. The muscular tension in the arterial wall T_{max} depends on η (which is the sum of the O_2 term shown and three similar terms for P_aCO_2 , arterial blood pressure and the demand parameter) in the following way:

$$T_{max} = T_{max0}(1 + k_{aut}\mu), \quad (2.3)$$

where T_{max0} is a constant, k_{aut} is a parameter representing the level of autoregulation, and μ is a sigmoidal function of η . An average vessel radius is calculated from the balance of pressures and tensions in the vessel wall. This in turn determines the conductance of the arterial/arteriolar tree via Poiseuille's law. A decrease in oxygen concentration therefore leads to an increase in the vessel radius and consequently an increase in blood volume and blood flow.

The venous compartment has a fixed resistance G_v . The pressure at its boundary with the arteries P_v is calculated by equating the cerebral blood flow (CBF) through the arteries and veins giving

$$P_v = \frac{GP_a + G_v P_{vs}}{G + G_v}, \quad (2.4)$$

where P_{vs} is the pressure in the venous sinuses. The normalized venous volume V_v is then calculated by

$$V_v = V_{v,n} + C_v(P_v - P_{v,n}), \quad (2.5)$$

where C_v is the venous compliance, including a normalizing factor.

All blood compartments have a fixed haemoglobin concentration $[Hb_{tot}]$. In each compartment, a fraction of this haemoglobin is oxygenated. These fractions are determined from the arterial oxygen saturation (a model input) and from the rate of oxygen transport. Dissolved oxygen from the capillaries diffuses directly to the mitochondrial compartment. The simulated NIRS haemoglobin signals ΔHHb and ΔHbO_2 are calculated from the concentrations of oxy and deoxyhaemoglobin in the arteries and veins as follows:

$$\begin{aligned} \Delta HHb &= V_{blood,n} \frac{1}{4} ([HHb_a] V_a + [HHb_v] V_v \\ &\quad - [HHb_a]_{n,V} V_{a,n} - [HHb_v]_{n,V} V_{v,n}) \end{aligned} \quad (2.6)$$

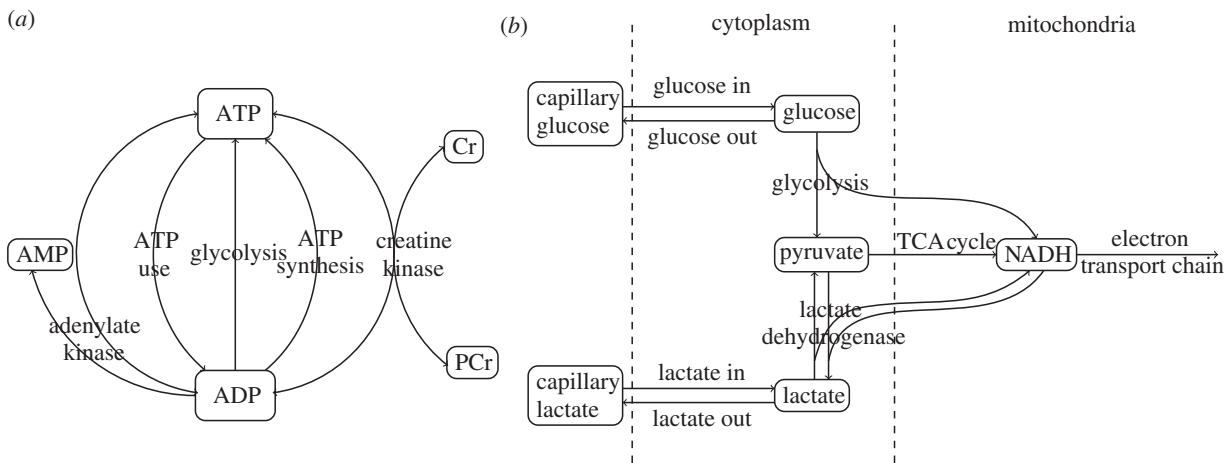


Figure 2. Diagrams of sections of the model that have been added to simulate MRS measured variables: (a) processes relating to ATP and (b) process relating to glycolysis, lactate and the TCA cycle.

and

$$\Delta HbO_2 = V_{\text{blood},n} \frac{1}{4} ([HbO_{2,a}]V_a + [HbO_{2,v}]V_v - [HbO_{2,a}]_n V_{a,n} - [HbO_{2,v}]_n V_{v,n}), \quad (2.7)$$

where $[HHb]$ and $[HbO_2]$ are the concentrations of deoxy- and oxyhaemoglobin in the blood, and subscripts a and v refer to the arterial and venous compartments.

2.2. Metabolism

The metabolic part of BrainSignals is limited to oxidative phosphorylation. Particular attention is given to the CCO complex. This part of BrainSignals has been preserved, and extended to include ATP use and production, glycolysis and lactate dynamics. Many of the additional processes take place in the cytoplasm. However, with the exception of protons, no transport processes between cytoplasm and mitochondria are explicitly modelled. All other metabolites are considered in only one of these compartments.

An overview of the processes in the model involving the adenosine phosphates is shown in figure 2a. ATP is produced by ATP synthase in the mitochondria and by glycolysis in the cytoplasm. The rate of flow of protons through ATP synthase depends on the electrochemical potential Δp and the Gibbs free energy of ATP hydrolysis ΔG as follows:

$$L_{CV} = L_{CV,\max} \left(\frac{1 - e^{-\theta}}{1 + r_{CV} e^{-\theta}} \right) \quad (2.8)$$

and

$$\theta = k_{CV} \left(\Delta p + \frac{\Delta G}{n_a F} \right),$$

where $L_{CV,\max}$ is the maximum rate of proton flow, r_{CV} is a parameter controlling the relative forward and backward rates, and F is the Faraday constant. This is altered from BrainSignals to give a direct dependence on the energy state. The parameter n_a is the number of protons required to phosphorylate one ATP, and includes the proton used in the exchange of ADP and ATP across the mitochondrial membrane. The Gibbs

free energy of ATP hydrolysis ΔG is calculated by

$$\Delta G = \Delta G^\circ + ZF \ln g_p \quad \text{and} \quad g_p = \frac{[ADP][P_i]}{[ATP]}, \quad (2.9)$$

where ΔG° is the standard Gibbs free energy of ATP hydrolysis, Z is a thermodynamic constant, and the ratio g_p is known as the phosphorylation potential. All concentrations are taken to be cytosolic concentrations. The ATP synthesis rate is equal to L_{CV}/n_a .

ATP use is modelled as a single Michaelis–Menten process with a half-maximum concentration ($k_{m,ATP}$) much lower than the normal ATP concentration. The reaction rate is therefore close to its maximum at normal ATP concentrations, and does not begin to decline significantly until ATP is low.

The final two processes influencing ATP concentration are buffering by phosphocreatine and AMP which occur with the following rates.

$$k_{PCr}[PCr][ADP] - k_{PCr}^-[ATP][Cr] \quad (2.10)$$

and

$$k_{AK} [ADP]^2 - k_{AK}^- [ATP][AMP]. \quad (2.11)$$

Both are modelled as mass action reactions and are assumed to reach equilibrium quickly. The ratio of forward and backward rate constants k_{PCr} and k_{PCr}^- is equal to the effective equilibrium constant for the reaction $K_{eq,PCr}$.

The remaining metabolic processes relate to glycolysis and lactate dynamics, and link these to the electron transport chain via the production of nicotinamide adenine dinucleotide (NAD) as shown in figure 2b. The net rate of glucose transport is

$$v_{glut} \left(\frac{[gluc_c]}{[gluc_c] + k_{glut}} - \frac{[gluc]}{[gluc] + k_{glut}} \right), \quad (2.12)$$

where $[gluc]$ is the glucose concentration in the cytoplasm and $[gluc_c]$ is the glucose concentration in the capillary, which is fixed. The maximum rate v_{glut} is set so that when glucose concentration is at its normal value $[gluc]_n$, the net transport rate is equal to the normal metabolic rate of glucose consumption

$\text{CMR}_{\text{gluc},n}$. The same form is used for lactate transport, with the net transport rate given by

$$v_{\text{MCT}} \left(\frac{[\text{lac}_c]}{[\text{lac}_c] + k_{\text{MCT}}} - \frac{[\text{lac}]}{[\text{lac}] + k_{\text{MCT}}} \right), \quad (2.13)$$

where $[\text{lac}]$ is the lactate concentration in the cytoplasm, and $[\text{lac}_c]$ is the capillary lactate concentration which is fixed. Transport of lactate between brain cells has been the subject of much recent modelling, owing to the interest in the neuron–lactate aspartate shuttle [36–38]. Neurons and astrocytes have different expression of the MCT family members, leading to different k_{MCT} [39]. In our model however, there is no distinction between the two cell types, and we use an intermediate value for k_{MCT} . The parameter v_{MCT} is calculated from the normal cerebral metabolic rate of lactate consumption $\text{CMR}_{\text{lac},n}$. If the model is to be at a steady state under normal conditions, the stoichiometry of the reactions gives an expression for $\text{CMR}_{\text{lac},n}$

$$\frac{1}{6} \text{CMRO}_2,n - \text{CMR}_{\text{gluc},n} = \frac{1}{2} \text{CMR}_{\text{lac},n}$$

Satisfying this equation with the chosen values for CMR_{gluc} and CMRO_2 results in a net production of lactate at baseline conditions.

Glycolysis is modelled as a single-stage Michaelis–Menten process with a rate dependent on glucose, ADP and P_i concentration. The maximum rate v_{glyc} is given by

$$v_{\text{glyc}} = v_{\text{glyc},n} \frac{I + 1}{1 + I([\text{ATP}] / [\text{ATP}]_n)([\text{AMP}]_n / [\text{AMP}])}, \quad (2.14)$$

where $v_{\text{glyc},n}$ is the normal maximum rate of glycolysis. This expression represents the regulation by ATP and AMP of phosphofructokinase, an enzyme that catalyses an important regulatory step in glycolysis [40]. The parameter I controls how much the rate of glycolysis can change for given changes in ATP and AMP concentrations.

The interconversion between pyruvate and lactate is modelled as a mass action reaction with rate

$$k_{\text{pl}}[\text{Py}] - k_{\text{pl}}^{-1}[\text{lac}]. \quad (2.15)$$

This reaction involves a proton, and the rate constants are related by

$$k_{\text{pl}} = \frac{[\text{H}^+]_n}{[\text{H}^+]_n} \frac{2\text{CMR}_{\text{lac},n} + k_{\text{pl}}^{-1}[\text{lac}]_n}{[\text{Py}]_n}. \quad (2.16)$$

The magnitude of the rate constants is set to give a ratio that adapts effectively instantly to pH changes. This reaction, and glycolysis, also involve NAD, but NAD in the cytoplasm is not modelled. However, the reactions cause a conversion between mitochondrial NAD and the reduced form of NAD (NADH) to give the correct stoichiometry.

The transformation of pyruvate to acetyl-CoA and the whole tricarboxylic acid (TCA) cycle are combined into a single reaction that consumes one molecule of pyruvate and produces five reducing equivalents.

These are all assumed to be NADH for simplicity. The rate is given by

$$\frac{v_{\text{TCA}}[\text{Py}][\text{NAD}]}{(k_{m,\text{tcaP}} + [\text{Py}])(k_{m,\text{tcaN}} + [\text{NAD}])}. \quad (2.17)$$

The k_m values were estimated from the detailed model of the TCA cycle by Wu *et al.* [32]. The k_m for pyruvate is small, since this model suggests that TCA cycle rate is not sensitive to pyruvate concentration unless it falls very low. The rate of the TCA cycle is also influenced by ATP and ADP concentrations. However, the main controlling factor is thought to be the NAD/NADH ratio [41].

The electron transport chain is described by three reactions. The first is the transfer of four electrons from NADH to the Cu_A centre of CCO. The second is the transfer of electrons from here to the cytochrome a_3 centre, and the final reaction is the reduction of oxygen to water. The rates are calculated based on thermodynamic principles. The rate of the third reaction, which is proportional to CMRO_2 , is given by

$$k_{3,0}[\text{O}_2][\text{a3r}]f(\Delta p), \quad (2.18)$$

where $k_{3,0}$ is a constant, f a function of the proton motive force Δp , $[\text{O}_2]$ the mitochondrial oxygen concentration and $[\text{a3r}]$ the concentration of reduced cytochrome a_3 .

2.3. Implementation

Model development, simulations and analysis were carried out using the BRAINCIRC modelling environment [42]. Steady-state simulations were used to analyse the model behaviour, and dynamic simulations were used to compare the model with experimental data.

3. RESULTS

The steady-state predictions by the model of CBF with changes in blood pressure, oxygen saturation and arterial carbon dioxide tension (P_{aCO_2}) are shown in figure 3. The changes in PCr and ATP concentration, CMRO_2 and ΔCu_A with arterial oxygen saturation are also shown. These simulations are compared with the equivalent simulations with the parameter values for adults shown in table 1.

3.1. Simulation of anoxia

The model was used to simulate a previous experiment involving brief anoxias in six newborn piglets [12]. The piglets were anaesthetized with isoflurane and artificially ventilated. Their inspired oxygen was reduced from 40 per cent to 0 for 105 s. After returning to 40 per cent O_2 for 10 min, the anoxia was repeated six times for each piglet. Mean arterial blood pressure (MAP) was monitored throughout, and continuous NIRS and ^{31}P MRS measurements were recorded. The results showed a decrease in ΔHbO_2 and increase in ΔHHb during anoxia. Immediately after anoxia there was an increase in total haemoglobin concentration indicating an increase in cerebral blood volume. There was a reduction of Cu_A during anoxia and a small

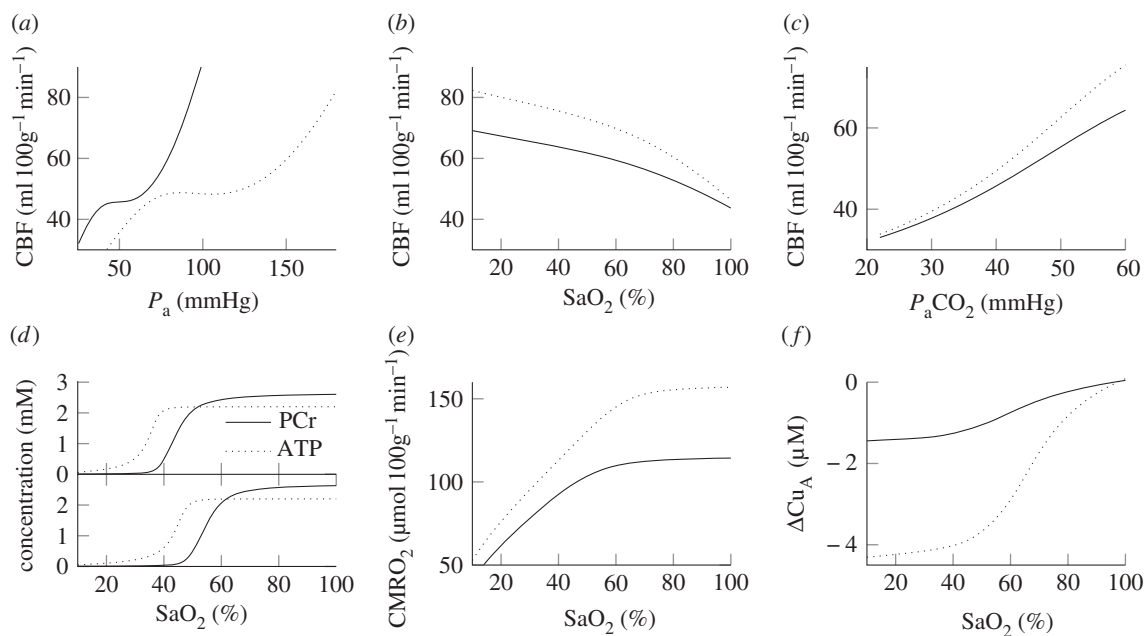


Figure 3. Steady-state simulations. (a–c) CBF versus arterial blood pressure, arterial oxygen saturation and arterial CO₂ pressure. Solid lines were simulated with the piglet parameter values and dotted lines with the adult values shown in table 1. (d) PCr and ATP concentration versus arterial oxygen saturation for (top) piglet parameter values and (bottom) adult parameter values. (e) and (f) CMRO₂ and change in Cu_A redox state versus arterial oxygen saturation for piglet parameter values (solid) and adult parameter values (dotted).

hyperoxidation upon reoxygenation. The MRS results showed a decrease in PCr and inorganic phosphate concentration, but no changes in ATP concentration were seen.

The MAP and arterial oxygen saturation (SaO₂) were used as inputs to the model, and its outputs were compared with the averaged NIRS and MRS measurements, as illustrated in figure 4.

Carbon dioxide levels were not reported during the challenge and assumed to remain constant. Oxygen saturation measurements were not available, so SaO₂ was estimated from the experimental protocol. This estimate is shown, along with the measured MBP, in figure 5. Comparisons between modelled and measured results showed some significant differences. By changing four parameters that were known to affect relevant parts of the model, the simulations were improved. These changes are listed in table 3 and are explained as follows:

- the autoregulation capacity in the model was decreased by reducing the parameter k_{aut} from 1.0 to 0.5. After this change, the maximum venous volume increase was approximately 45 per cent. The effect of this change on the autoregulation curve is shown in figure 6. The change in CBF as a percentage of baseline between 30 and 70 mmHg increased from 0.8% mmHg⁻¹ with $k_{aut} = 1.0$ to 2.1% mmHg⁻¹ with $k_{aut} = 0.5$. The improvement in the simulation of total haemoglobin concentration changes is shown in figure 7;
- the glycolysis rate was made more sensitive to changes in AMP and ATP concentration by increasing the parameter I from 3 to 50. This resulted in an approximately sevenfold increase in glycolysis rate

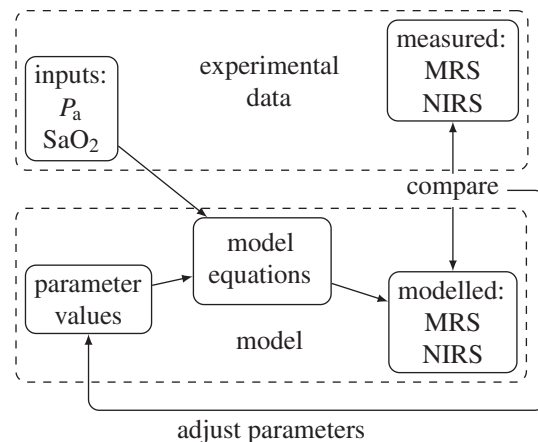


Figure 4. Flow chart showing the modelling process.

during anoxia. Also, when $I = 50$, the PCr concentration at the end of anoxia was 55 per cent of its baseline value compared with 25% when $I = 3$; the normal ratio of PCr to P_i was increased from 1.5 to 2.7. In the model, if ATP concentration is constant, changes in PCr and P_i concentration are equal and opposite (ignoring AMP which is present only at very small concentrations). The experimental results therefore require a ratio of [PCr]_n to [P_i]_n of 2.7. With this ratio, the model will accurately simulate the P_i measurements providing the PCr measurements are accurately simulated; the normal NAD/NADH ratio was decreased from 9 to 1.5. This resulted in a decrease in the rate of Cu_A reduction.

The modelled and measured results after implementing these changes are shown in figure 8. The model's

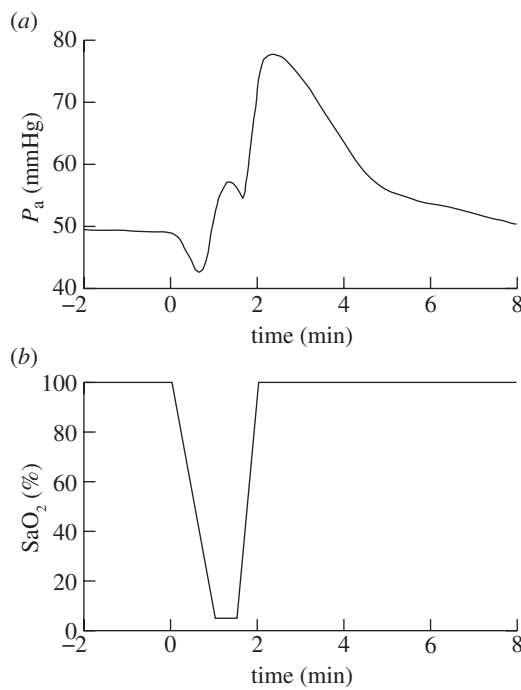


Figure 5. (a) Arterial blood pressure and (b) arterial oxygen saturation used as model inputs to simulate anoxia [12]. Blood pressure was taken from the measurements from one piglet. SaO_2 was estimated from the experimental protocol.

Table 3. Table of model parameters that were changed to improve the model simulations of anoxia.

parameter	default value	changed value
$[PCr]_n/[P_i]_n$	1.5	2.7
I	3	50
k_{aut}	1.0	0.5
$[NAD]_n/[NADH]_n$	9.0	1.5

predictions for lactate concentration and $CMRO_2$ are shown in figure 9. $CMRO_2$ was predicted to decrease to 15% of its baseline value during anoxia and increase to 108% during reoxygenation.

In addition to these changes, the model was altered to explore the simulation of the Cu_A redox state. This was done to investigate the hyperoxidation seen following anoxia, which is seen in the data but is not well understood. Initially, equation (2.18) was changed to

$$k_{3,0} \frac{[O_2]}{k + [O_2]} (k + [O_2]_n) [a3r] f(\Delta p), \quad (3.1)$$

where $k = 5 \mu M$. The model was then further changed such that there was no dependence of ATP synthesis rate on phosphorylation potential by replacing ΔG with its normal value in equation (2.8). The results of these changes are shown in figure 10. When equation (3.1) is used, the simulation of ΔCu_A is significantly improved as SaO_2 begins to drop (although the simulation is slightly worse at lower SaO_2). Also, the magnitude of hyperoxidation of Cu_A during recovery is decreased. When, in addition, the dependence of

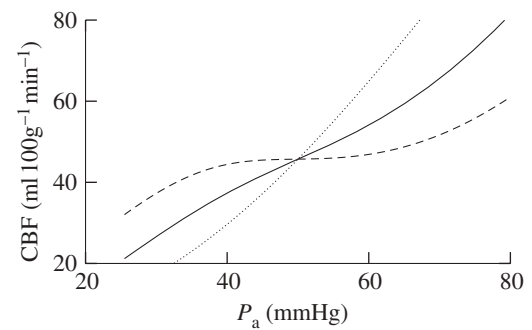


Figure 6. Steady-state CBF versus mean arterial blood pressure after the parameter changes shown in table 3 but with $k_{aut} = 1$ (dashed line) 0.5 (solid line) and 0 (dotted line). CBF changes (in the range 30–70 mmHg) are 0.8, 2.1 and 3.8%/mmHg, respectively.

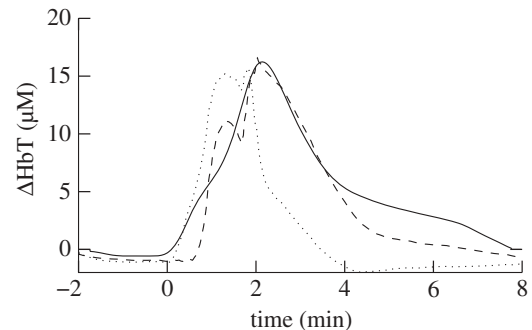


Figure 7. Measured (solid line) total change in haemoglobin concentration ($\Delta HHb + \Delta HbO_2$) and simulated with $k_{aut} = 0.5$ (dashed line) and $k_{aut} = 1.0$ (dotted line) with the parameter value changes shown in table 3.

ATP synthesis rate on phosphorylation potential is removed, no hyperoxidation is seen.

4. DISCUSSION

The model has been applied successfully to simulate oxygenation and metabolic changes in the brains of newborn piglets during anoxia. It correctly predicted no significant changes in ATP concentration throughout the experiment. To simulate the other measured signals, changes to the original model were required. These changes offer an insight into the physiological interpretation of the experimental results as discussed below. In addition, the model allows predictions of variables that are more difficult to measure, including $CMRO_2$ and lactate concentration.

During recovery from anoxia, a large increase in MAP accompanied by an increase in $[HbO_2]$ was measured. As there was not a corresponding reduction in $[HHb]$, this implies an increase in cerebral blood volume. The model suggests that this hyperaemia cannot be attributed to changes in the arterial volume alone. A dilation of the cerebral arteries to this extent would be predicted to cause a several-fold increase in CBF, which, unless accompanied by a corresponding increase in $CMRO_2$, would lead to a decrease in $[HHb]$ via a washout effect. It is more likely, therefore, that

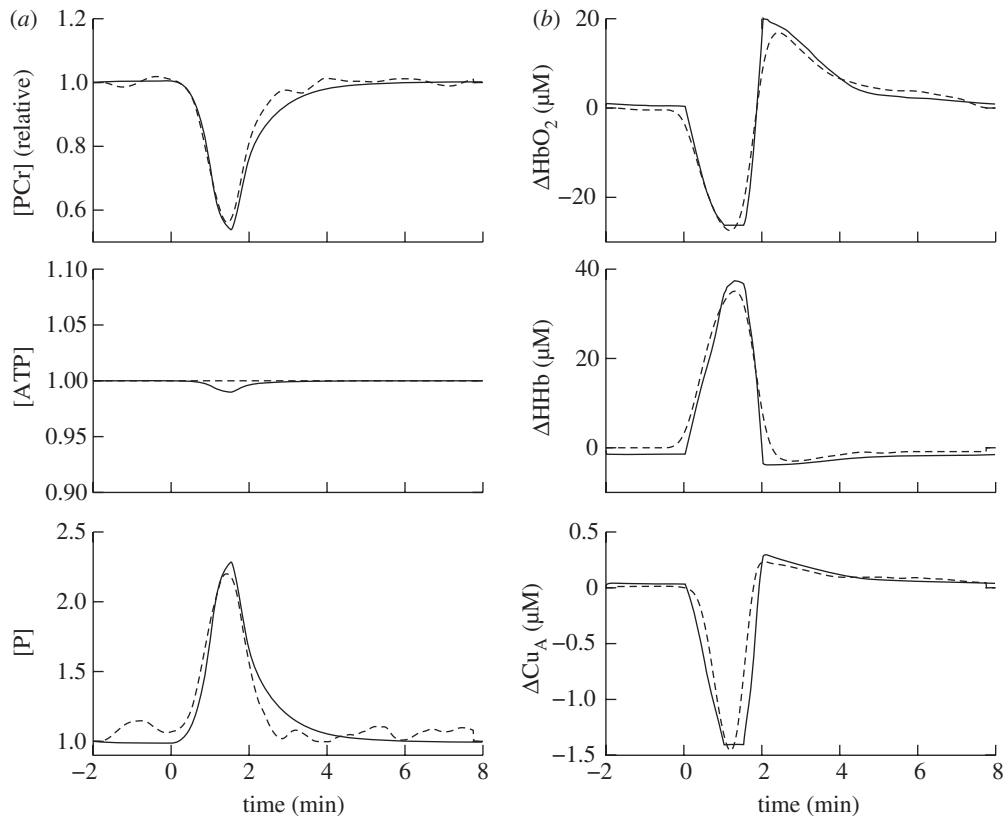


Figure 8. Model simulations (solid line) compared with measurements (dashed line) from NIRS (b) and MRS (a) during anoxia in piglets, taken from Springett *et al.* [12]. Parameter values for the model were set to those in table 3.

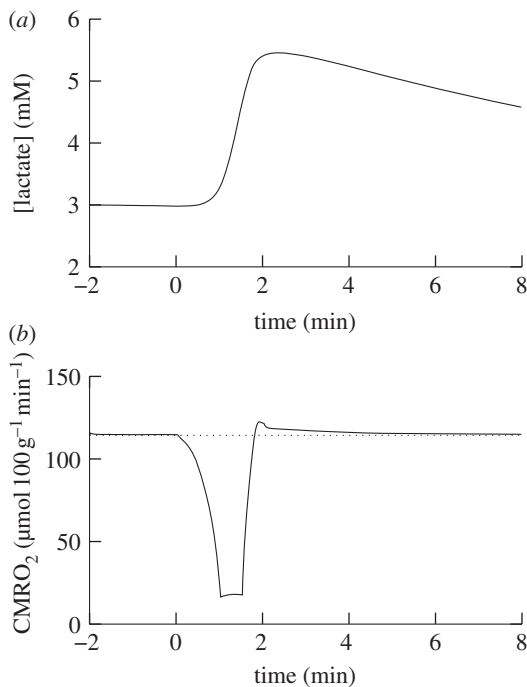


Figure 9. (a) Model predictions of lactate concentration and (b) CMRO₂ with normal CMRO₂ shown as dotted during anoxia.

the increased blood volume following anoxia has a significant venous contribution, which is driven by the increase in blood pressure. However, the autoregulation behaviour of the model causes changes in arterial

pressure of this magnitude to be damped by changes in arterial resistance before they are felt at the veins. A reduction of the parameter k_{aut} from 1.0 to 0.5 reduced this cancelling effect, and so led to a better replication of the observed hyperaemia. Previous studies in piglets have found that CBF does not change in the range of 50–80 mmHg [43–45]. However, these studies used piglets older than 24 h. In one study involving piglets of different ages, it was found that for piglets less than 4 days old, the average change in CBF as blood pressure was varied was 1.1%/mmHg, whereas for piglets older than 4 days old it was 0%/mmHg [46]. The interpretation of the anoxia measurements using our model suggests that cerebral autoregulation was impaired or not fully developed in these newborn piglets.

The relationship between PCr and ATP concentration in the model as oxygen saturation falls shows the expected buffering of ATP by PCr, with ATP not decreasing until PCr is low. The model predicts that ATP concentration will begin to decrease when SaO_2 falls below 40 per cent. However, the model predicted a drop in PCr concentration during anoxia larger than that observed. Increasing the parameter I allowed a greater increase in glycolysis rate, and therefore a greater rate of ATP synthesis during anoxia. This glycolysis rate could not be sustained for longer anoxias, because the model predicts that glucose is used faster than its maximum rate of transport into the cell. The value of I was increased from 3 to 50. Above this value, there is almost no further change in glycolysis rate, because changes in ATP and AMP

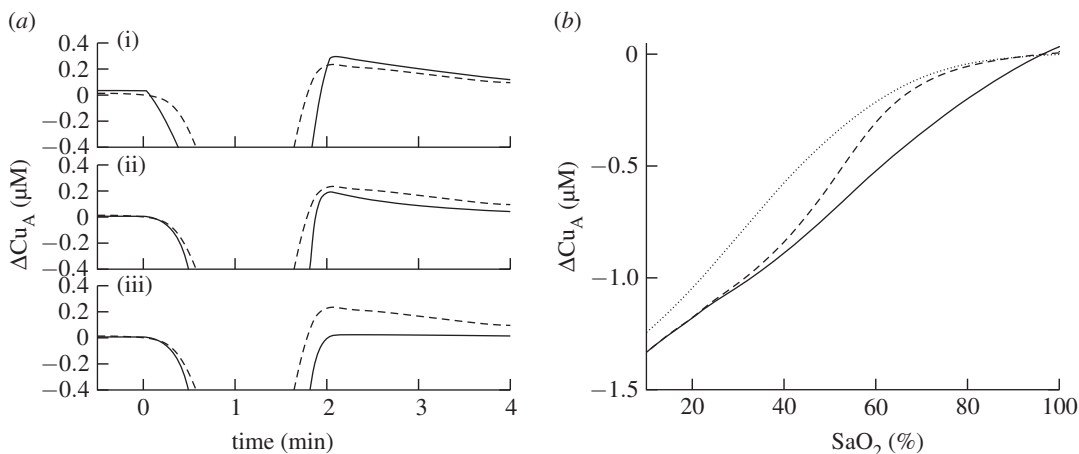


Figure 10. (a) Comparison of measured Cu_A signal (dashed) with modelled Cu_A signal (solid) for (from top to bottom) (i). The model with its default equations, and parameter values from table 3 (ii). As (i), but with an altered CMRO_2 dependence on oxygen (equation (2.18) replaced with equation (3.1)) (iii). As (ii), but with no dependence on phosphorylation potential of ATP synthesis rate (ΔG replaced with its normal value in equation (2.8)). (b) ΔCu_A vs oxygen saturation at the onset of anoxia for measured data (dashed) model as in (i) on left (solid) and model as in (ii) on left (dotted).

concentrations become limiting. For large I , the glycolysis rate in the model increased approximately sevenfold. This is greater than the fivefold increase calculated to occur in foetal rats during ischaemia [47]. It should be noted that the extent of PCr concentration decrease in the model is also sensitive to the normal PCr concentration [$\text{PCr}]_n$. There are two features of particular interest in the Cu_A experimental results: the delay between the decrease in HbO_2 , and the reduction of Cu_A , and the hyperoxidation of Cu_A during recovery. The former is not reproduced by the model in its original form, but the latter is. It has been observed previously in piglets that Cu_A redox state is not affected by mild hypoxia [48] i.e. CCO has a low apparent k_m for oxygen. A similar effect has also been observed in adult rats [49,50], but not in adult humans [51,52]. The mechanisms for this effect are unknown, and it does not emerge from our alterations of the BrainSignals model to simulate the neonatal piglet brain. But, when included directly in the model, it improved the simulation of Cu_A reduction at the onset of anoxia. As expected, it also decreased the magnitude of Cu_A hyperoxidation following anoxia, since this is partly caused by the increased oxygen tension at the mitochondria as a consequence of the increased oxygen delivery. An oxidation is still seen however, because the increased concentrations of ADP and P_i during and following anoxia increase the rate of ATP synthesis via equations (2.8) and (2.9). The proton motive force across the mitochondrial membrane is decreased which increases CMRO_2 and, with the parameter values used, results in an oxidation of Cu_A . If this dependency on phosphorylation potential is removed, no oxidation is seen. This supports the suggestion of Springett *et al.* [12] when reporting the experimental results, that the hyperoxidation was a result of an increased CMRO_2 . A Cu_A hyperoxidation following anoxia was also observed in an earlier study [53]. The authors suggest that a pH drop could partly be responsible for the oxidation via a direct affect of pH on Cu_A . There is no mechanism for this effect in our model, although a

small change in pH was observed following anoxia, as measured by MRS.

Another possible explanation for the oxidation is a decrease in the substrate supply to the TCA cycle. Our model suggests the opposite is true for pyruvate, whose concentration increases during anoxia, and takes several minutes to return to normal. However, there is an increase in NADH/NAD ratio which will tend to decrease the rate of the TCA cycle; but this appears to have only a small effect on the oxidation of Cu_A . The NAD/NADH ratio does however have a significant effect on the rate of reduction of Cu_A . Although changes in mitochondrial NADH concentration can be measured by fluorescence, the NAD/NADH ratio is difficult to measure *in vivo* [54]. Estimates of this ratio differ, for example in rat liver cells a ratio of 5–10 was measured [55], but in myocytes isolated from newborn piglets a ratio of 1.2 was found [56]. We found a decrease in the model's normal NAD/NADH ratio from 9 to 1.5 led to the simulated rate of Cu_A reduction matching the experimental rate. However, there are other factors that affect this rate, including the form of the TCA cycle rate dependence on NAD/NADH ratio, and the sensitivity of the reactions of the electron transport chain to changes in the proton gradient. This part of our model requires further investigation.

There are some limitations of our model. In general, we wish to keep the model as simple as possible, while still accurately replicating experimental results in a way that is representative of the underlying physiology. We believe that this allows a greater understanding of the model's behaviour. However, some aspects may have been oversimplified. In particular, it may be necessary to model NAD, NADH and pH in the cytoplasm. The ratio of NAD to NADH in the cytoplasm is much larger than in the mitochondria [55]. Changes in these variables affect the lactate to pyruvate ratio, and the rate of glycolysis. Also, we have not distinguished between astrocytes and neurons. Their different functions are important when considering

lactate dynamics. Finally, for the anoxia experiment simulated here, the assumption of constant arterial CO₂ concentration is unlikely to be correct. CO₂ changes have an important effect on blood flow, and may have affected the simulation of the NIRS haemoglobin signals.

We have used a physiological approach to construct our model. The main strength of this type of modelling is that it allows hypotheses to be generated and tested. However, it can lead to more complex models, and this makes it more difficult to analyse. Therefore, some components that have been simplified are treated phenomenologically. In this paper, we relied on knowledge of the model and experimentation to identify parameters with important effects. In the future, we will implement a more rigorous sensitivity analysis to analyse the effects of all parameters on particular model outputs. We are currently using the model to simulate MRS and NIRS measurements during HI in piglets. These measurements have complex relationships with one another, and we will use the model to help understand them in the context of our biological knowledge. We will also use it to simulate new treatments such as xenon-augmented hypothermia which is being investigated in our group [57].

The authors would like to thank The Wellcome Trust (088429/Z/09/Z) for the financial support of this work.

REFERENCES

- 1 Erecinska, M., Cherian, S. & Silver, I. A. 2004 Energy metabolism in mammalian brain during development. *Progr. Neurobiol.* **73**, 397–445. (doi:10.1016/j.pneurobio.2004.06.003)
- 2 Tsuji, M., Allred, E., Jensen, F. & Holtzman, D. 1995 Phosphocreatine and ATP regulation in the hypoxic developing rat brain. *Dev. Brain Res.* **85**, 192–200. (doi:10.1016/0165-3806(94)00213-J)
- 3 Tichauer, K. M., Elliott, J. T., Hadway, J. A., Lee, D. S., Lee, T. & Lawrence, K. S. 2010 Using near-infrared spectroscopy to measure cerebral metabolic rate of oxygen under multiple levels of arterial oxygenation in piglets. *J. Appl. Physiol.* **109**, 878–885. (doi:10.1152/japplphysiol.01432.2009)
- 4 Vannucci, R. C. 1990 Experimental biology of cerebral hypoxia–ischemia: relation to perinatal brain damage. *Pediatr. Res.* **27**, 317. (doi:10.1203/00006450-199004000-00001)
- 5 Roohey, T., Raju, T. N. K. & Moustogiannis, A. N. 1997 Animal models for the study of perinatal hypoxic–ischemic encephalopathy: a critical analysis. *Early Hum. Dev.* **47**, 115–146. (doi:10.1016/S0378-3782(96)01773-2)
- 6 Banaji, M., Tachtsidis, I., Delpy, D. & Baigent, S. 2005 A physiological model of cerebral blood flow control. *Math. Biosci.* **194**, 125–173. (doi:10.1016/j.mbs.2004.10.005)
- 7 Banaji, M., Mallett, A., Elwell, C. E., Nicholls, P. & Cooper, C. E. 2008 A model of brain circulation and metabolism: NIRS signal changes during physiological challenges. *PLoS Comput. Biol.* **4**, 1000212. (doi:10.1371/journal.pcbi.1000212)
- 8 Owen-Reece, H., Smith, M., Elwell, C. E. & Goldstone, J. C. 1999 Near infrared spectroscopy. *Brit. J. Anaesth.* **82**, 418–426.
- 9 Wolf, M., Ferrari, M. & Quaresima, V. 2007 Progress of near-infrared spectroscopy and topography for brain and muscle clinical applications. *J. Biomed. Opt.* **12**, 062104. (doi:10.1117/1.2804899)
- 10 Wolf, M. & Greisen, G. 2009 Advances in near-infrared spectroscopy to study the brain of the preterm and term neonate. *Clin. Perinatol.* **36**, 807–834. (doi:10.1016/j.clp.2009.07.007)
- 11 van der Graaf, M. 2009 *In vivo* magnetic resonance spectroscopy: basic methodology and clinical applications. *Eur. Biophys. J.* **39**, 527–540. (doi:10.1007/s00249-009-0517-y)
- 12 Springett, R., Wylezinska, M., Cady, E. B., Cope, M. & Delpy, D. T. 2000 Oxygen dependency of cerebral oxidative phosphorylation in newborn piglets. *J. Cereb. Blood Flow Metab.* **20**, 280–289. (doi:10.1097/00004647-200002000-00009)
- 13 Springett, R. 2001 Precise measurement of cerebral blood flow in newborn piglets from the bolus passage of indocyanine green. *Phys. Med. Biol.* **46**, 2209. (doi:10.1088/0031-9155/46/8/312)
- 14 Cooper, C. E. & Springett, R. 1997 Measurement of cytochrome oxidase and mitochondrial energetics by near-infrared spectroscopy. *Phil. Trans. R. Soc. Lond. B* **352**, 669–676. (doi:10.1098/rstb.1997.0048)
- 15 Springett, R., Newman, J., Cope, M. & Delpy, D. T. 2000 Oxygen dependency and precision of cytochrome oxidase signal from full spectral NIRS of the piglet brain. *Am. J. Physiol. Heart Circ. Physiol.* **279**, H2202–H2209.
- 16 Brown, D. W., Hadway, J. & Lee, T. 2003 Near-infrared spectroscopy measurement of oxygen extraction fraction and cerebral metabolic rate of oxygen in newborn piglets. *Pediatr. Res.* **54**, 861–867. (doi:10.1203/01.PDR.0000090928.93045.BE)
- 17 Lossec, G., Lebreton, Y., Hulin, J. C., Fillaut, M. & Herpin, P. 1998 Age-related changes in oxygen and nutrient uptake by hindquarters in newborn pigs during cold-induced shivering. *Exp. Physiol.* **83**, 793–807.
- 18 Soul, J. S., Taylor, G. A., Wypij, D., Duplessis, A. J. & Volpe, J. J. 2000 Noninvasive detection of changes in cerebral blood flow by near-infrared spectroscopy in a piglet model of hydrocephalus. *Pediatr. Res.* **48**, 445. (doi:10.1203/00006450-200010000-00005)
- 19 Roth, K. & Weiner, M. W. 1991 Determination of cytosolic ADP and AMP concentrations and the free energy of ATP hydrolysis in human muscle and brain tissues with 31P NMR spectroscopy. *Magn. Resonance Med.* **22**, 505–511. (doi:10.1002/mrm.1910220258)
- 20 Corbett, R. J., Laptook, A. R., Garcia, D. & Ruley, J. I. 1993 Energy reserves and utilization rates in developing brain measured *in vivo* by 31P and 1H nuclear magnetic resonance spectroscopy. *J. Cereb. Blood Flow Metab.* **13**, 235–246. (doi:10.1038/jcbfm.1993.29)
- 21 Aubert, A., Costalat, R. & Valabregue, R. 2001 Modelling of the coupling between brain electrical activity and metabolism. *Acta Biotheoretica* **49**, 301–326. (doi:10.1016/S1053-8119(01)92610-2)
- 22 Rosenkrantz, T. S., Kubin, J., Mishra, O. P., Smith, D. & Delivoria-Papadopoulos, M. 1996 Brain cell membrane Na⁺,K⁺-ATPase activity following severe hypoxic injury in the newborn piglet. *Brain Res.* **730**, 52–57. (doi:10.1016/0006-8993(96)00430-1)
- 23 Penrice, J. 1997 Proton magnetic resonance spectroscopy of the brain during acute hypoxia–ischemia and delayed cerebral energy failure in the newborn piglet. *Pediatr. Res.* **41**, 795. (doi:10.1203/00006450-199706000-00001)
- 24 Brand, M., Pakay, J., Ocloo, A., Kokoszka, J., Wallace, D., Brookes, P. & Cornwall, E. 2005 The basal proton conductance of mitochondria depends on adenine nucleotide

- translocase content. *Biochem. J.* **392**, 353. (doi:10.1042/BJ20050890)
- 25 Korzeniewski, B. & Zoladz, J. A. 2001 A model of oxidative phosphorylation in mammalian skeletal muscle. *Biophys. Chem.* **92**, 17–34. (doi:10.1016/S0301-4622(01)00184-3)
- 26 Lawson, J. W. & Veech, R. L. 1979 Effects of pH and free Mg²⁺ on the *keq* of the creatine kinase reaction and other phosphate hydrolyses and phosphate transfer reactions. *J. Biol. Chem.* **254**, 6528–6537.
- 27 Flecknell, P. A., Wootton, R. & John, M. 1983 Cerebral blood flow and cerebral metabolism in normal and intrauterine growth retarded neonatal piglets. *Clin. Sci.* **64**, 161–165.
- 28 Gruetter, R., Novotny, E. J., Boulware, S. D., Rothman, D. L., Mason, G. F., Shulman, G. I., Shulman, R. G. & Tamborlane, W. V. 1992 Direct measurement of brain glucose concentrations in humans by ¹³C NMR spectroscopy. *Proc. Natl Acad. Sci. USA* **89**, 1109–1112. (doi:10.1073/pnas.89.3.1109)
- 29 Pourcyrous, M., Leffler, C. W., Bada, H. S., Korones, S. B. & Busija, D. W. 1994 Cerebral blood flow responses to indo-methacin in awake newborn pigs. *Pediatr. Res.* **35**, 565. (doi:10.1203/00006450-199405000-00007)
- 30 Ursino, M. & Lodi, C. A. 1998 Interaction among autoregulation, CO₂ reactivity, and intracranial pressure: a mathematical model. *Am. J. Physiol.* **274**, 1715.
- 31 Edvinsson, L., Mackenzie, E. T. & McCulloch, J. 1992 *Cerebral blood flow and metabolism*. New York, NY: Raven Press.
- 32 Wu, F., Yang, F., Vinnakota, K. C. & Beard, D. A. 2007 Computer modeling of mitochondrial tricarboxylic acid cycle, oxidative phosphorylation, metabolite transport, and electrophysiology. *J. Biol. Chem.* **282**, 24525–24537. (doi:10.1074/jbc.M701024200)
- 33 Berg, J. M., Tymoczko, J. L. & Stryer, L. 2011 *Biochemistry: international edition*, 7th edn. San Francisco, CA: W. H. Freeman.
- 34 Moroz, T. BrainPiglet. See <http://www.ucl.ac.uk/medphys/research/borl/nirs/mrs>.
- 35 Ito, H., Kanno, I. & Fukuda, H. 2005 Human cerebral circulation: positron emission tomography studies. *Ann. Nucl. Med.* **19**, 65–74. (doi:10.1007/BF03027383)
- 36 Aubert, A. & Costalat, R. 2005 Interaction between astrocytes and neurons studied using a mathematical model of compartmentalized energy metabolism. *J. Cereb. Blood Flow Metab.* **25**, 1476–1490. (doi:10.1038/sj.jcbfm.9600144)
- 37 DiNuzzo, M., Mangia, S., Maraviglia, B. & Giove, F. 2010 Changes in glucose uptake rather than lactate shuttle take center stage in subserving neuroenergetics: evidence from mathematical modeling. *J. Cereb. Blood Flow Metab.* **30**, 586–602. (doi:10.1038/jcbfm.2009.232)
- 38 Cloutier, M., Bolger, F. B., Lowry, J. P. & Wellstead, P. 2009 An integrative dynamic model of brain energy metabolism using *in vivo* neurochemical measurements. *J. Comput. Neurosci.* **27**, 391–414. (doi:10.1007/s10827-009-0152-8)
- 39 Simpson, I. A., Carruthers, A. & Vannucci, S. J. 2007 Supply and demand in cerebral energy metabolism: the role of nutrient transporters. *J. Cereb. Blood Flow Metab.* **27**, 1766–1791. (doi:10.1038/sj.jcbfm.9600521)
- 40 Siesjö, B. K. 1978 *Brain energy metabolism*. New York, NY: Wiley.
- 41 LaNoue, K., Nicklas, W. J. & Williamson, J. R. 1970 Control of citric acid cycle activity in rat heart mitochondria. *J. Biol. Chem.* **245**, 102–111.
- 42 Banaji, M. BRAINCIRC home page. See <http://braincirc.sourceforge.net/>.
- 43 Laptook, A., Stonestreet, B. S. & Oh, W. 1982 Autoregulation of brain blood flow in the newborn piglet: regional differences in flow reduction during hypotension. *Early Hum. Dev.* **6**, 99–107. (doi:10.1016/0378-3782(82)90063-9)
- 44 Chemtob, S., Beharry, K., Rex, J., Varma, D. & Aranda, J. 1990 Prostanoids determine the range of cerebral blood flow autoregulation of newborn piglets. *Stroke* **21**, 777–784. (doi:10.1161/01.STR.21.5.777)
- 45 Brady, K. M., Lee, J. K., Kibler, K. K., Easley, R. B., Koehler, R. C. & Shaffner, D. H. 2008 Continuous measurement of autoregulation by spontaneous fluctuations in cerebral perfusion pressure. *Stroke* **39**, 2531–2537. (doi:10.1161/STROKEAHA.108.514877)
- 46 Haaland, K., Karlsson, B., Skovlund, E., Lagercrantz, H. & Thoresen, M. 1995 Postnatal development of the cerebral blood flow velocity response to changes in CO₂ and mean arterial blood pressure in the piglet. *Acta Paediatrica* **84**, 1414–1420. (doi:10.1111/j.1651-2227.1995.tb13579.x)
- 47 Duffy, T. E. 1975 Carbohydrate and energy metabolism in perinatal rat brain: relation to survival in anoxia. *J. Neurochem.* **24**, 271. (doi:10.1111/j.1471-4159.1975.tb11875.x)
- 48 Tsuji, M., Naruse, H., Volpe, J. & Holtzman, D. 1995 Reduction of cytochrome aa3 measured by near-infrared spectroscopy predicts cerebral energy loss in hypoxic piglets. *Pediatr. Res.* **37**, 253. (doi:10.1203/00006450-199503000-00001)
- 49 Hoshi, Y., Hazeki, O., Kakihana, Y. & Tamura, M. 1997 Redox behavior of cytochrome oxidase in the rat brain measured by near-infrared spectroscopy. *J. Appl. Physiol.* **83**, 1842–1848.
- 50 Cooper, C. E., Matcher, S. J., Wyatt, J. S., Cope, M., Brown, G. C., Nemoto, E. M. & Delpy, D. T. 1994 Near-infrared spectroscopy of the brain: relevance to cytochrome oxidase bioenergetics. *Biochem. Soc. Trans.* **22**, 974–980.
- 51 Tisdall, M. M. & Smith, M. 2007 Multimodal monitoring in traumatic brain injury: current status and future directions. *Brit. J. Anaesth.* **99**, 61–67. (doi:10.1093/bja/aem143)
- 52 Tachtsidis, I., Tisdall, M. M., Leung, T. S., Pritchard, C., Cooper, C. E., Smith, M. & Elwell, C. E. 2009 Relationship between brain tissue haemodynamics, oxygenation and metabolism in the healthy human adult brain during hyperoxia and hypercapnia. *Adv. Exp. Med. Biol.* **645**, 315–320. (doi:10.1007/978-0-387-85998-9_47)
- 53 Quaresima, V., Springett, R., Cope, M., Wyatt, J. T., Delpy, D. T., Ferrari, M. & Cooper, C. E. 1998 Oxidation and reduction of cytochrome oxidase in the neonatal brain observed by *in vivo* near-infrared spectroscopy. *Biochim. Biophys. Acta* **1366**, 291–300. (doi:10.1016/S0005-2728(98)00129-7)
- 54 Mayevsky, A. & Chance, B. 2007 Oxidation–reduction states of NADH *in vivo*: from animals to clinical use. *Mitochondrion* **7**, 330–339. (doi:10.1016/j.mito.2007.05.001)
- 55 Williamson, D. H., Lund, P. & Krebs, H. A. 1967 The redox state of free nicotinamide-adenine dinucleotide in the cytoplasm and mitochondria of rat liver. *Biochem. J.* **103**, 514–527.
- 56 Livingston, B. E., Altschuld, R. A. & Hohl, C. M. 1996 Metabolic compartmentalization in neonatal swine myocytes. *Pediatr. Res.* **40**, 59–65. (doi:10.1203/00006450-199607000-00011)
- 57 Faulkner, S. et al. 2011 Xenon augmented hypothermia reduces early lactate/N-acetylaspartate and cell death in perinatal asphyxia. *Ann. Neurol.* **70**, 133–150. (doi:10.1002/ana.22387)